Dual-Scan Photoacoustic Tomography for the Imaging of Vascular Structure on Foot

Chuqin Huang, Yanda Cheng, Wenhan Zheng, Robert W. Bing, Huijuan Zhang, Isabel Komornicki, Linda M. Harris, Praveen R. Arany, Saptarshi Chakraborty, Qifa Zhou, *Fellow, IEEE*, Wenyao Xu, *Senior Member, IEEE*, and Jun Xia, *Member, IEEE*

***Abstract*—Chronic leg ulcers are affecting approximately 6.5 million Americans, and they are associated with significant mortality, reduced quality of life, and high treatment costs. Since many chronic ulcers have underlying vascular insufficiency, accurate assessment of tissue perfusion is critical to treatment planning and monitoring. This study introduces a dual-scan photoacoustic (PA) tomography (PAT) system that can simultaneously image the dorsal and plantar sides of the foot to reduce imaging time. To account for the unique shape of the foot, the system employs height-adjustable and articulating baseball stages that can scan along the foot's contour. In vivo results from healthy volunteers demonstrate the system's ability to acquire clear images of foot vasculature, and results from patients indicate that the system can image patients with various ulcer conditions. We also investigated various PA features and examined their correlation with the foot condition. Our preliminary results indicate that vessel sharpness, occupancy, intensity, and density could all be used to assess tissue perfusion. This research demonstrated the potential of PAT for routine clinical tissue perfusion assessment.**

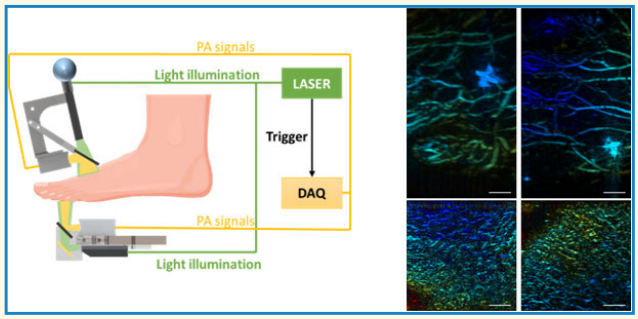

***Index Terms*—Chronic leg ulcers, foot imaging, PA tomography (PAT), peripheral vascular disorders, photoacoustic (PA).**

I. Introduction

CHRONIC leg ulcers are commonly associated with peripheral vascular disorders and affect approximately 6.5 million Americans [1], [2], [3]. Patients with ulcers commonly suffer from decreased mobility and lower quality of life [2]. Revascularization surgery is one of the most effective treatments for ischemia-related foot ulcers, as it restores blood flow and perfusion to the ulcer region. Thus, the ability to monitor the change in perfusion before and after surgery is essential in determining surgical success.

However, current clinical tests fail to meet this need [4]. For instance, ankle-brachial index (ABI) and toe-brachial index (TBI) cannot provide information on perfusion conditions of a specific region; handheld Doppler Ultrasound has limitations due to its low sensitivity to the microvasculature [5]; photoplethysmography (PPG) is affected by skin conditions and its readings cannot be mapped to a single vessel [6]; transcutaneous oxygen ($TcPO_2$) pressure requires a long acquisition time (larger than 30 min) and has not been shown to accurately assess perfusion related healing [7]; and X-ray CT angiogram and ICG-based near-infrared fluorescence angiography have ionizing radiation or need contrast agent injection and are not appropriate for monitoring perfusion over time.

Photoacoustic (PA) tomography (PAT) is an emerging imaging modality based on the PA effect [8]. The light energy is transformed into heat during the light absorption

Manuscript received 18 May 2023; accepted 30 May 2023. Date of publication 5 June 2023; date of current version 13 December 2023. This work was supported by the National Institute of Health under Grant R01EB029596 and Grant R01EB028978. *(Chuqin Huang and Yanda Cheng are co-first authors.) (Corresponding author: Jun Xia.)*

This work involved human subjects or animals in its research. Approval of all ethical and experimental procedures and protocols was granted by the Institutional Review Boards of the University at Buffalo under Protocol No. STUDY00001165, and performed in line with established standards within the institution.

Chuqin Huang, Yanda Cheng, Wenhan Zheng, Robert W. Bing, Huijuan Zhang, and Jun Xia are with the Department of Biomedical Engineering, University at Buffalo, The State University of New York, Buffalo, NY 14228 USA (e-mail: junxia@buffalo.edu).

Isabel Komornicki and Linda M. Harris are with the Department of Surgery, University at Buffalo, The State University of New York, Buffalo, NY 14228 USA.

Praveen R. Arany is with the Department of Oral Biology, Biomedical Engineering, and Surgery, University at Buffalo, Buffalo, NY 14228 USA.

Saptarshi Chakraborty is with the Department of Biostatistics, University at Buffalo, Buffalo, NY 14228 USA.

Qifa Zhou is with the Department of Biomedical Engineering, University of Southern California, Los Angeles, CA 90007 USA.

Wenyao Xu is with the Department of Computer Science and Engineering, University at Buffalo, Buffalo, NY 14228 USA.

Digital Object Identifier 10.1109/TUFFC.2023.3283139

Highlights

- **In this study, a dual-scan PAT system has been developed to scan both sides of the foot simultaneously.**
- **PA images have been acquired from multiple patients with foot ulcers and we identified PA features that are correlated with tissue perfusion.**
- **The proposed PAT system has great potential for the assessment of foot ulcers.**

in tissue. Meanwhile, mechanical waves, which are generated by the thermoelastic expansion of the tissue, are detected by ultrasonic probes [9]. High-resolution PA images of light absorption can be formed by back-projecting PA signals. PAT overcomes the diffusion limit of light and generates high-resolution images in optical diffusive regimes, as acoustic scattering is much weaker than that of light in tissue [9]. For perfusion assessment, a major PA contrast is hemoglobin, and its concentration and distribution are correlated with blood perfusion. Compared to other optical imaging methods for foot assessment, PA imaging has unique advantages. For instance, direct eye visualization is the most common technique in wound assessment, but it cannot provide functional or depth information. Optical fluorescence imaging has also been used for perfusion assessment [7], [10], however, it needs contrast agent injection. Multispectral imaging is another emerging technique [11]. While it provides functional information on blood oxygenation, it cannot reveal the vasculature and depth information. In contrast, PAT enables label-free 3-D imaging of hemoglobin distribution, allowing for safe assessment of the blood perfusion after revascularization surgery.

Over the past few years, various PAT systems have been proposed for imaging foot ulcers. For instance, Yang et al. [12], [13] devised a real-time PA/Ultrasound (US) system with an arc-shaped concave transducer array and compared the PA signal intensity with and without occlusion. Taruttis et al. [14] proposed a handheld multispectral optoacoustic tomography (MSOT) with a concave transducer array for imaging both major and microvasculature on the foot, providing images of hemoglobin oxygen saturation and pulsation. Mantri et al. [15] utilized an LED-based PA system with a linear transducer array to monitor the peripheral hemodynamic response to changes in blood pressure in healthy volunteers and patients undergoing hemodialysis. However, all these systems could only image a cross section, and the selection of the cross section is operator-dependent. Recently, Choi et al. [16] developed a 3-D PA/US multistructural quantitative imaging platform with a linear transducer array and the system provides volumetric and multiparametric information about the foot. A potential concern is that the system requires the foot to be fully immersed in water, which could pose a challenge for patients with wounds. Additionally, the system necessitates a longer scanning time as it needs a prescan for height estimation. Lee et al. [17] demonstrated a compact handheld 3-D PA/US scanner that does not need water immersion. However, the motion artifact might impact the imaging quality. Nagae et al. [18] built a 3-D limb imaging system using a hemispherical detector array. However, the system is relatively bulky and expensive due to the transducer design. In addition, positioning of the foot is not very convenient. Previously, our group also introduced a 3-D PAT system for wound assessment, and we demonstrated preliminary results from patients. However, similar to all 3-D PAT systems mentioned above, it can only image one side of the foot, while ulcers might occur at multiple locations [19].

Here, we introduce a dual-scan 3-D PAT system for imaging the vascular structure of the foot. The system is capable of imaging both the dorsal and plantar sides of the foot simultaneously to reduce imaging time. The whole system is built on a cart and takes very little clinical space. To account for the height change on the dorsal side of the foot, we also integrated a laser distance sensor into the motion control system. The performance of our system is demonstrated through phantom imaging and human tests. Our results indicate that the system has a high potential for clinical translation.

II. Methods

A. System Design

The proposed system is comprised of two scanning subsystems, as shown in Fig. 1(a). The top subsystem images the instep of the foot, while the bottom subsystem scans the plantar side. The light source is a portable Nd:YAG laser (Big Sky Laser) operating at 10 Hz with a pulsewidth of about 8 ns and a wavelength of 1064 nm. The laser output is coupled to a bifurcated fiber bundle (Dolan-Jenner Industries) for light delivery to both top and bottom subsystems. PA signals from both subsystems are captured by a 256-channel data acquisition (DAQ) unit (PhotoSound Technologies Inc.) operating at a 40-MHz sampling rate. Synchronization of data capturing and laser pulse is achieved by trigger signals from the laser. The entire system is installed on a mobile cart (McMaster Inc.), as shown in Fig. 1(b). An optical breadboard (Thorlabs, Inc.) is mounted on the lower level of the cart as the base of the system. The water tank for the bottom subsystem is fixed to the breadboard, whereas the top one is mounted on two position slides (McMaster Inc.), so the top water tank can be moved up and down to fit different foot sizes. Both water tanks are made with clear polycarbonate sheets (McMaster Inc.) and the imaging windows are sealed with 0.001″ plastic films.

The scanning head of the top subsystem consists of a customized linear-array transducer (Imasonic SAS, France) with 128 elements and 2.25-MHz central frequency (named as L2), one of the bifurcated fiber bundle output (3-inch line output), a high-performance cold mirror (Edmund Optics Inc.), and a 3-D-printed base. The transducer elements were designed by scaling down the frequency of a clinical L7-5 transducer from 5 to 2.25 MHz. It has an 86-mm total length to cover the region of interest (ROI) on foot, and each element is

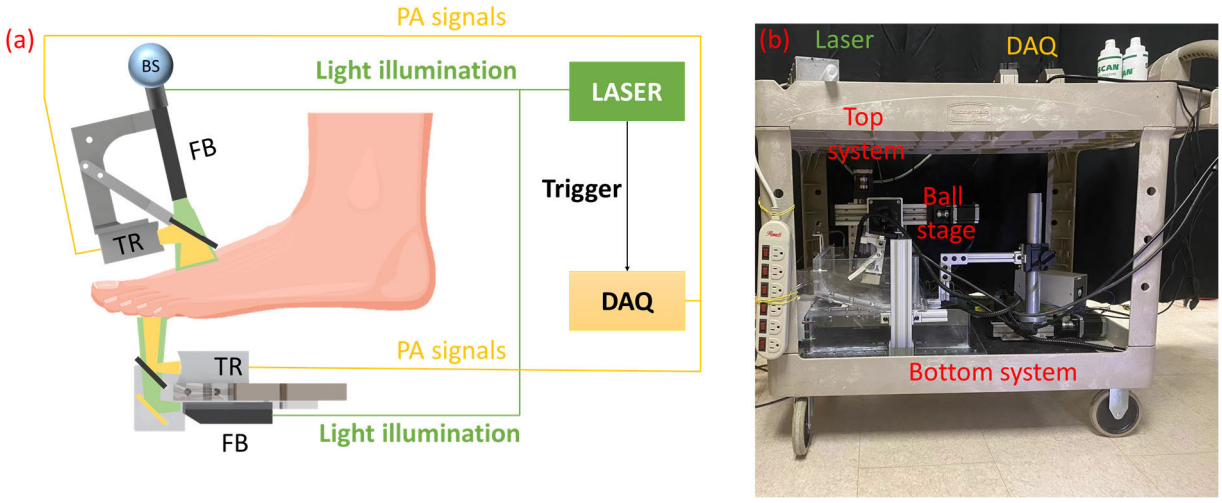

Fig. 1. Experimental setup of the dual-scan imaging system. (a) Schematic drawing of the dual-scan PAT system. The light transmission is marked in green, while the acoustic propagation is labeled in yellow. BS: Ball stage; FB: fiber bundle; TR: transducer. (b) Photograph of the system. Most equipment is installed on a cart except the portable laser.

curved to achieve acoustic focusing without using a lens. The transducer and fiber bundle head are placed vertically to each other as shown in Fig. 1(a), and the cold mirror is attached at 45° to the fiber bundle. This design achieves coplanar light illumination and acoustic detection, offering optimum imaging depth [20]. The scanning head is installed on an articulating baseball stage (Thorlabs Inc.), allowing easy positioning of the head to align with the foot surface. The ball stage is further mounted on two translation stages, which are used for scanning and height adjustment, respectively.

As the bottom scanning head is completely immersed in water, a double mirror structure shown in Fig. 1(a) is utilized to achieve the coplanar light delivery and acoustic receiving [21]. A high-performance hot mirror (>95% reflection at 1064 nm, Edmund Optics Inc.) is mounted in front of the fiber bundle to reflect the light. Another cold mirror is placed parallel to the hot mirror as shown in Fig. 1(a), which enables over 90% transmission at 1064 nm and reflects the acoustic waves to the transducer. The bottom linear-array transducer has 128 elements with 5-MHz central frequency and 50-mm lateral length. A higher frequency transducer is used at the bottom as vessels are smaller on the plantar side of the foot. The scanning head is connected to a translation stage and driven by a stepper motor to perform linear scanning.

B. Foot Coupling

Before placing the foot on the bottom water tank, we attach a small medical tape on the skin for better correlation of the PA imaging region with the photographs. The tape has a cross-shaped black mark, which can be visualized in PA. Then, we apply ultrasound gel on the plantar side of the foot filling the gaps between the toes to enhance acoustic coupling. For patients with foot ulcers, we used sterilized clear Gel (AquaSonic clear, Parker Laboratories, Inc.) to reduce the risk of infection. The plantar side of the patient's foot is mostly flat, so the bottom water tank has a flat imaging window covered by a plastic membrane [Fig. 2(a)].

The top imaging window has a slope to account for the height difference between the toes and ankle. Based on prior research [22], the average foot size length of an elderly American is 255.9 mm and the average instep height is 114 mm, leading to a 24° slope. We chose to design a 15° tilted imaging window, as the smaller angle will improve coupling. Once the patient places their foot on the bottom water tank, more ultrasound gel is applied on the instep side. Then, the top water tank is lowered for coupling. The movement of the top water tank is manually controlled by two translation stages. As the top water tank is lowered, the foot instep surface is slightly compressed by the membrane on the water tank to improve acoustic coupling.

The limited view natural of a linear array indicates that the optimal performance of the system is achieved when the array surface is aligned with the object. As the foot instep surface is not flat, we used the articulating platform to manually control transducer positioning before scanning. As depicted in Fig. 2(a), the rotation angle is determined manually based on the shape of the foot instep. After the foot coupling procedures have been completed, we can begin scanning with the motion control system.

C. Motion Control

During the experiment, both the top and bottom transducers move simultaneously at a constant scanning speed of 1 mm/s. The height change in the foot instep also brings a challenge in scanning. To ensure that the transducer focus always stays around the skin surface, we used a laser distance sensor (TOF 10102, OCESTORE, US) to estimate the instep height, which is used to guide the scanning. As shown in Fig. 2(a), the laser distance sensor is attached to the edge of the top water tank. The laser distance sensor measures and records the instep ankle height. Then, the information is sent to the Arduino program to calculate the endpoint position for the top transducer. This design allows the travel path to vary with ankle heights to ensure that the transducer's focus stays near the foot surface.

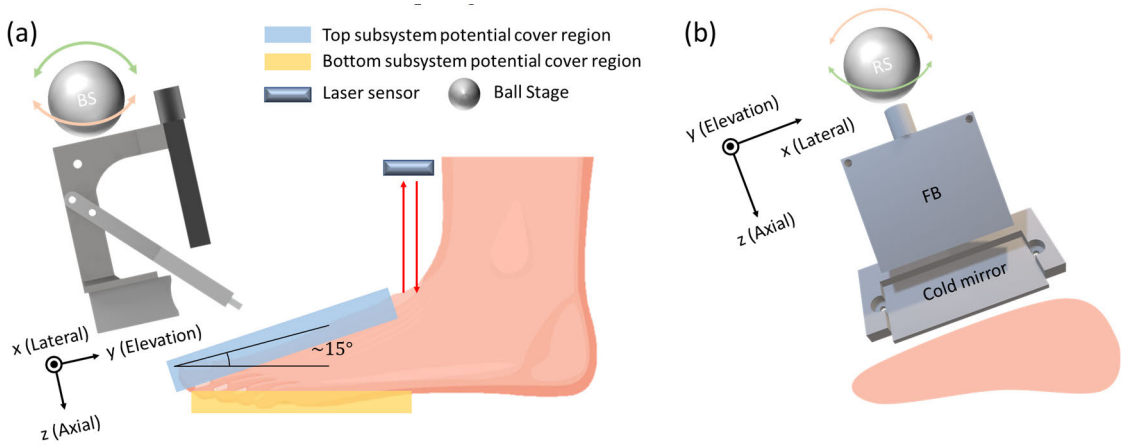

Fig. 2. Schematic drawings of the top and bottom scanning schemes. (a) Schematic drawing in axial-elevation view of the transducer. The laser distance sensor is mounted close to the ankle to measure the distance from the sensor to the skin surface. The potential scanning regions are marked with blue and yellow for the top and bottom systems, respectively. The scanner is rotated via the ball stage in the axial-elevation plane to align with the foot. (b) Schematic drawing in the axial–lateral view of the transducer. The transducer is positioned parallel to the lateral direction, covering from the right (big toe) to the left (small toe). The scanner can also be manually rotated in the axial–lateral plane to fit the curve of the foot.

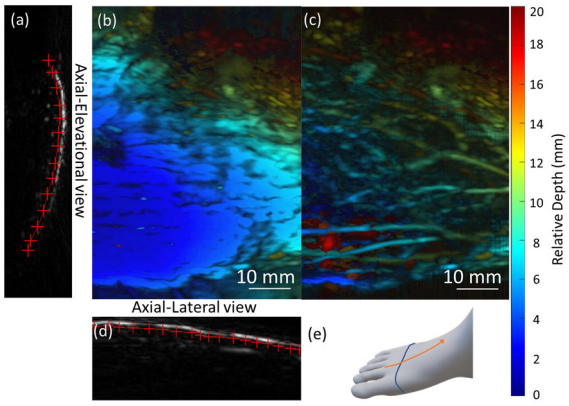

Fig. 3. Demonstration of the skin removal algorithm. (a) Manual selection of the skin region in axial–lateral cross-sectional view. (b) PA depth-encoded maximum amplitude projection (MAP) image of the subject's foot. The skin signal has strong intensity, making it hard to see vessels beneath the skin. (c) PA depth-encoded MAP image after the skin removal algorithm. The vessels can now be clearly visualized. (d) Manual selection of the skin region in axial-elevation cross-sectional view. (e) Schematic drawing of the foot and the curves used to mark the skin. The blue curve shows the cross-sectional profile of the foot and the orange curve shows the height change of the foot.

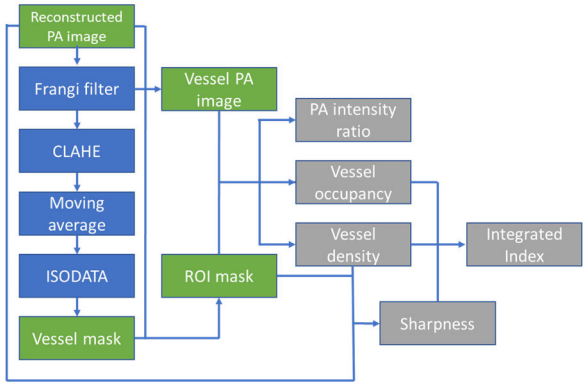

Fig. 4. Flowchart of the feature extraction procedure.

D. Image Reconstruction and Processing

As the Photosound system does not offer real-time display, we transferred raw channel data into the computer for offline processing and reconstruction. We first filter the data by a bandpass filter (1–5 MHz for the top and 3–7 MHz for the bottom) to eliminate noise and then use the back project algorithm to reconstruct the PA image [23]. The 2-D image frames are then stacked along the scanning direction to form a 3-D image. A wavelet filter is further used to remove electromagnetic interference noises, which is shown as stripes in the reconstructed images [24]. For better visualization, we use the depth-encoded maximum projection image (MAP) to display the 3-D image in 2-D.

We also noticed that the PA surface signal could be high in subjects with dark skin color. Therefore, we developed a skin removal algorithm to reveal the underlying vessels. The algorithm requires the operator to manually pick multiple points in reconstructed data to label the border between the skin and tissue, as shown in Fig. 3. The operation is performed on the axial–lateral plane first to extract the lateral contour of the foot [Fig. 3(a) and the blue line in Fig. 3(e)], and then the same operation is applied on the axial-elevation plane to get the elevation contour of the foot [Fig. 3(d) and the orange line in Fig. 3(e)]. A 3-D skin map is then generated by sweeping the lateral contour along the elevation curve as shown in Fig. 3(e). The skin map will be projected to the reconstruction space to mark the regions where the signal will be removed. Fig. 3(b) shows a PA image of a patient with dark skin, where strong surface signals can be observed. Fig. 3(c) shows the PA image after skin removal, where the subdermal vasculature structure can be visualized. The manually picked points are shown in Fig. 3(a) and (d).

To quantify PA features of tissue perfusion, we extract the vessels in the PAT images for further analysis. The detailed steps are listed in Fig. 4. We first apply the Frangi filter [25] on the grayscale MAP images to improve the vessel contrast and then use the contrast-limited adaptive histogram equalization (CLAHE) to further enhance signals from deeper

depths [26]. The resulting image is smoothed with a moving average filter to remove noise [27]. Then, segmentation is performed on the postprocessed image to create a vessel mask, based on the threshold obtained by the ISODATA clustering algorithm [27], [28].

Once the vessel mask is acquired, we compute the convex hull using MATLAB's built-in function, bwconvhull, to label the ROI. Meanwhile, the marker area (on the medical tape) is also identified and will be excluded from the analysis. Four PA-related features are studied to evaluate the perfusion condition within these areas. The first feature is the PA intensity ratio, which is calculated as the ratio of the mean intensity of PA signals within the vessel mask of the healthy foot to that of the foot with ulcers. This feature is related to the total hemoglobin concentration. The second feature is blood vessel occupancy (VO), which is evaluated by calculating the ratio of vessel region to the whole ROI. The third feature is vessel density (VD), which is related to VO. In contrast, VD quantifies the number of vessels instead of the area of vessels. To do so, we extract the centerline of the vessels using the MATLAB built-in function bwskel [29], [30]. The VD is then calculated by dividing the number of vessel pixels by the ROI. The last feature is vessel sharpness, as quantified based on (1), shown below [31]:

$$\text{Sharpness} = \frac{\sum \sqrt{G_x^2 + G_y^2}}{\text{Area} \times \text{Vessel density}} \tag{1}$$

where G_x and G_y are the gradients of the image along the horizontal and vertical directions, respectively, and Area is the total number of pixels in the ROI. Chronic wounds are often associated with leaking vessels [32], which might cause blurry edges of vessels. For better comparison across features, the calculated PA intensity is divided by 10^5, and the sharpness index is multiplied by 10^2 in this work.

We also investigated the possibility of integrating different vessel features into a single index. The proposed equation is shown in (2). Here, the coefficient for each feature is the reciprocal of the average indices from healthy volunteers. The coefficients are used to normalize the features. As the vasculature on the instep and sole exhibit different characteristics, the coefficients are determined independently for the top and bottom systems [33].

$$\text{Integrated index} = \begin{cases} 2.68 \times VO + 1.37 \times \text{sharpness} \\ +0.52 \times VD, & \text{for top} \\ 2.07 \times VO + 0.83 \times \text{sharpness} \\ +0.27 \times VD, & \text{for bottom.} \end{cases} \tag{2}$$

III. Results

A. Resolution Quantification

To quantify system resolution, we used a 0.2-mm width cross-line phantom made by a laser printer. The phantom was placed on a 3-D-printed foot to mimic the experimental environments. A ballistic gel pad was placed between the foot and phantom for better coupling. The distance from the phantom to the transducer is around 4 cm, which is the focal distance of the transducer. PA images of the phantom from the top and bottom systems are shown in Fig. 5(a) and (b), respectively. The spatial resolution was quantified based on the full-width at half-maximum (FWHM) of the reconstructed image. The pixels used for resolution quantification are marked in the PA reconstructed images, where the red line marks lateral and the green line labels elevation. The lateral resolution was quantified to be 0.77 and 0.54 mm for the top system and bottom systems as shown in Fig. 5(c) and (d), respectively. As indicated in Fig. 5(e) and (f), the elevation resolutions are 1.20 and 0.87 mm for the top system and bottom systems, respectively.

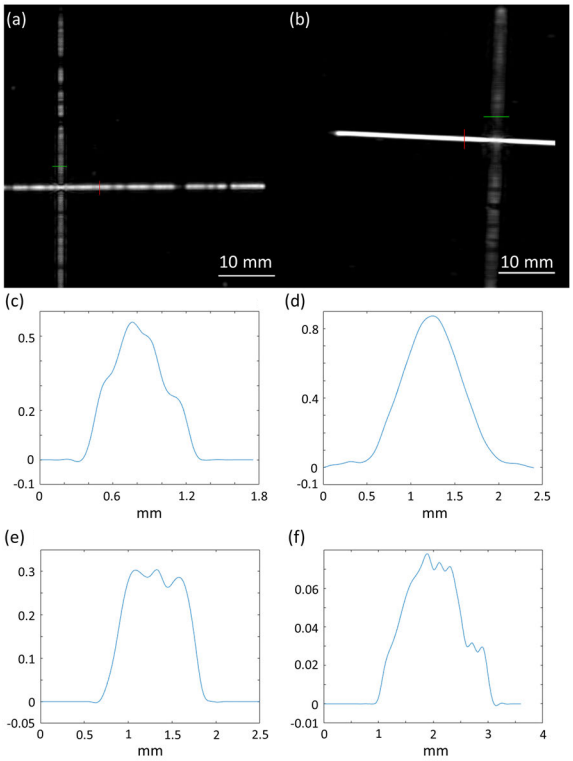

Fig. 5. Quantification of the system's spatial resolution. (a) Maximum amplitude projection (MAP) image of the cross-line phantom acquired by the bottom system. (b) MAP image of the cross-line phantom acquired by the top system. The resolution is quantified by FWHM. (c)–(d) The lateral resolutions are 0.54 and 0.77 mm in the bottom and top systems, respectively. (e)–(f) The elevation resolutions are 0.87 and 1.20 mm in the bottom and top systems, respectively.

B. Healthy Volunteer Results

1) Volunteer Characteristics: The methodology, data, and consent forms for healthy human subjects used in this research were approved by the IRB committee at the University at Buffalo. We recruited four healthy volunteers, and all volunteers signed the experiment consent form to collect foot image data. None of the volunteers has foot ulcers or health problems related to the foot.

2) Human Foot Imaging Protocols: Before clinical testing, we tested system usability and robustness with healthy

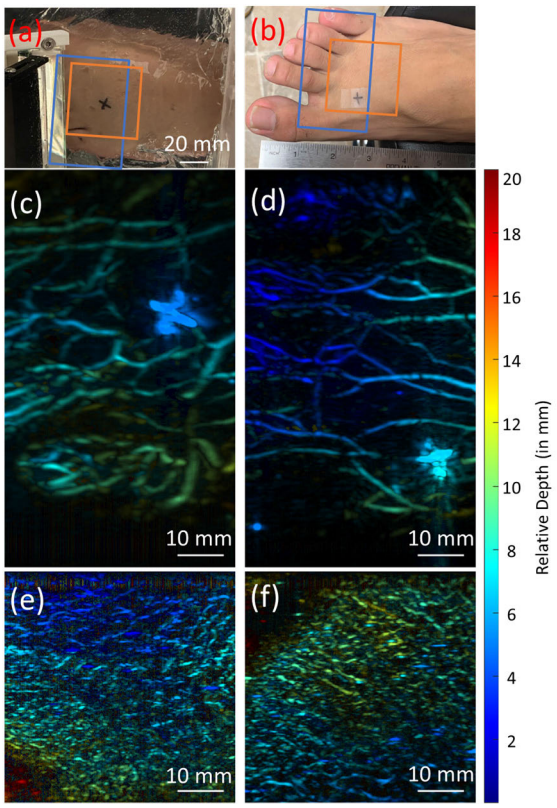

Fig. 6. In vivo results from two healthy volunteers. (a) Photograph of the left foot of healthy volunteer 1 (HV01). (b) Photograph of the right foot of healthy volunteer 2 (HV02). (c) PA depth-encoded MAP image of the dorsal side of the left foot from HV01. (d) PA depth-encoded MAP image of the dorsal side of the right foot from HV02. (e) PA depth-encoded MAP image of the plantar side of the left foot from HV01. (f) PA depth-encoded MAP image of the plantar side of the right foot from HV02. The scanning regions of the top system and bottom system are labeled with blue and orange rectangles, respectively.

volunteers. The scanning length of the foot instep was 50 mm along the elevation direction from toes to ankle, with a step size of 0.1 mm. The lateral imaging length covered 86 mm from the big toe to the small toe. The scan range of the bottom was 50 mm from toes to arch, with a step size of 0.1 mm. The lateral imaging length covered 50 mm from the big toe to the small toe. The imaging acquisition time was 50 s, and the entire imaging session took only 20 min from the subject's arrival to dismissal.

3) In Vivo Results From the Healthy Volunteer: Fig. 6(a) and (b) shows the results of two volunteers with a foot size of 10 and 8.5 (US size), respectively. Two groups of scanning were performed on both the dorsal side and plantar side of the foot, and the approximate scanning regions are labeled with blue (for the top system) and orange rectangles (for the bottom system). Depth-encoded MAP images are shown in Fig. 6(c)–(f). The results indicate that our system is capable of providing vascular information on both sides of the foot simultaneously. The vessel features are evaluated for healthy subjects, and the results are listed in Table I. Based on our results, the VD, sharpness, and occupancy are all higher at the plantar side of the foot, while PA intensity is higher at the dorsal side, as the dorsal skin is thinner which attenuates less light [34].

TABLE I
VESSEL FEATURES EXTRACTED FROM THE HEALTHY VOLUNTEERS

Foot	Top		Bottom	
	L (HV01)	R (HV02)	L (HV01)	R (HV02)
Vessel Occupancy	0.39	0.34	0.53	0.47
Sharpness x10^2	0.49	0.65	0.99	1.07
Vessel Density	2.05	1.82	4.85	3.81
Integrated Index	2.70	2.64	3.23	2.89

C. Patient Imaging Results

The proposed system is also tested in the clinic (UBMD vascular surgery, Amherst, NY, USA) by imaging patients with ulcers. The inclusion criterion is any person 18 years of age or older with one or multiple chronic wounds on the foot which is related to arterial perfusion insufficiency or gangrene. Pregnant women and adults unable to consent are excluded from the study. The ABI and TBI measurements are conducted before PA experiments by the clinicians.

Patient 1 is a 68-year-old male with a femoral artery aneurysm and gangrene on the toe of the left foot. PA imaging is performed on both left and right feet for comparison. As shown in Fig. 7(a) and (b), the scanning region (calibrated based on the marker) is labeled with a blue rectangle for the top systems. A chronic ulcer is observed on the bottom of the left foot, as shown in Fig. 7(c). The ulcer has mostly healed based on clinical records. PA imaging results are shown in Fig. 7(d)–(g). The ABI and TBI, acquired before the PA experiments, are listed in Fig. 7(d) and (e), showing that the perfusion condition is similar in both feet. The vessel features are quantified, and the results are listed in Table II. It can be seen that the index of most features on the top of the right foot (healthier foot) is higher than the left one, which agrees with the foot condition and ABI and TBI test results. For the bottom imaging results, the left foot has a lower integrated index than the right one, though the VO and VD show different trends.

Patient 2 is a 52-year-old male with right tranmetatarsal amputation due to ulcers as shown in Fig. 8(a) and (b). In addition, the subject has an open wound on the side of the left foot. PA imaging result from the dorsal side of the left (open wound observed) foot is shown in Fig. 8(c), while the dorsal PA image of the foot with amputation is shown in Fig. 8(d). Similar to patient 1, we quantified the vessel features and listed the results in Table II. For most vessel features, the foot with better perfusion condition (left) has much higher values than the amputated one (right). Our system needs further development to acquire the bottom image with this special wound case.

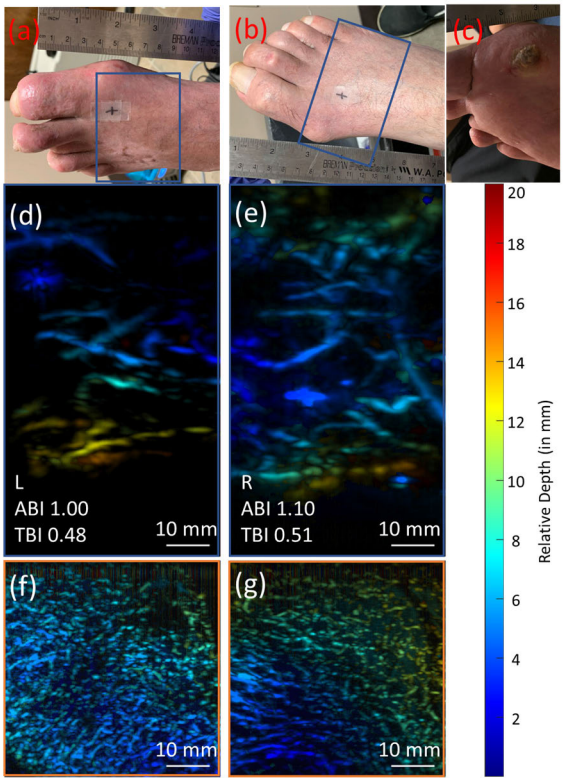

Fig. 7. In vivo results from the patient with an ulcer at the plantar side of the left foot. (a) Photograph of the subject's left foot. (b) Photograph of the subject's right foot. (c) Photograph of the ulcer, which is located on the dorsal side of the left foot. (d) PA depth-encoded MAP image of the dorsal side of the left foot. (e) PA depth-encoded MAP image of the dorsal side of the right foot. (f) PA depth-encode MAP image of the plantar side of the left foot. (g) PA depth-encoded MAP image of the plantar side of the right foot. The imaging region for the top system is labeled with a blue rectangle.

TABLE II
VESSEL FEATURES EXTRACTED FROM PATIENTS 1 AND 2. PATIENT 1 HAS A WOUND ON THE LEFT FOOT (MARKED IN RED). PATIENT 2 HAS A WOUND (AMPUTATION) ON THE RIGHT FOOT (MARKED IN RED)

Patient Number	Patient 1				Patient 2	
Foot	Top		Bottom		Top	
	L	R	L	R	L	R
PA intensity ratio	1.39		1.24		1.96	
Vessel occupancy	0.33	0.41	0.41	0.31	0.39	0.15
Sharpness x10^2	0.47	0.46	1.15	1.78	0.30	0.16
Vessel density	1.56	1.92	3.54	2.67	2.10	0.83
Integrated index	2.34	2.73	2.76	2.84	2.50	1.03

Patient 3 is an 84-year-old patient with chronic ulcers and toe amputation. The photographs of the foot and results from the PAT system are shown in Fig. 9. The scanning window is set to cover the region with amputation [Fig. 9(a) and (b)]. The vessel features are evaluated within the region and the results are shown in Table III. The indices of the amputated foot (left) are smaller than the healthier one (right),

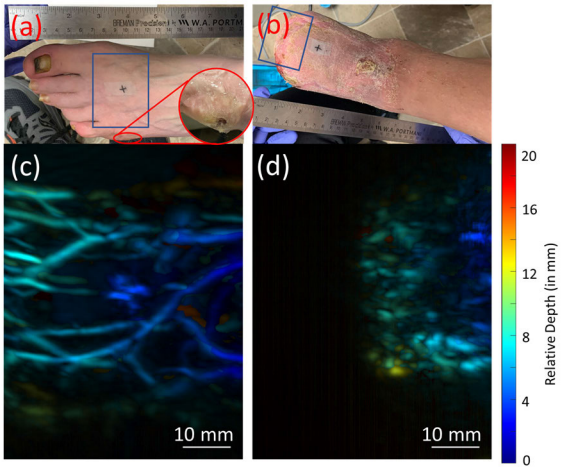

Fig. 8. In vivo results of the patient with multiple ulcers on the right foot. The front of the right foot was amputated. (a) Photograph of the patient's left foot. A close look from the side view shows an open wound. (b) Photograph of the patient's right foot, which has been amputated, and multiple ulcers are observed. (c) PA depth-encoded MAP image of the dorsal side of the left foot. (d) PA depth-encoded MAP image of the dorsal side of the right foot.

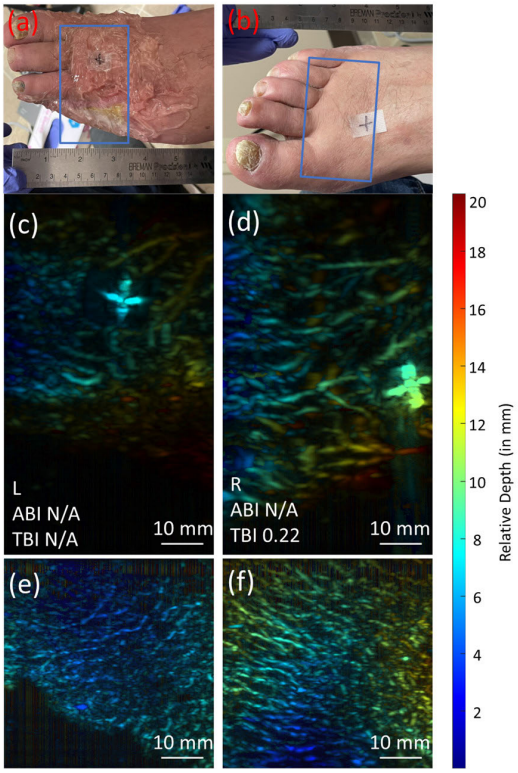

Fig. 9. In vivo results of a patient with wounds on the left foot. (a) Photograph of the left foot. Two toes were amputated due to chronic ulcers. (b) Photograph of the right foot (no open wound was observed). (c) PA depth-encoded MAP image of the dorsal side of the left foot. (d) PA depth-encoded MAP image of the dorsal side of the right foot. (e) PA depth-encoded MAP image of the plantar side of the left foot. (f) PA depth-encoded MAP image of the plantar side of the right foot. The scanning regions of the top system are labeled with blue rectangles in photographs.

except for the VO index on the dorsal side. A 3-D rendering of the foot vasculature can be found in supplementary materials.

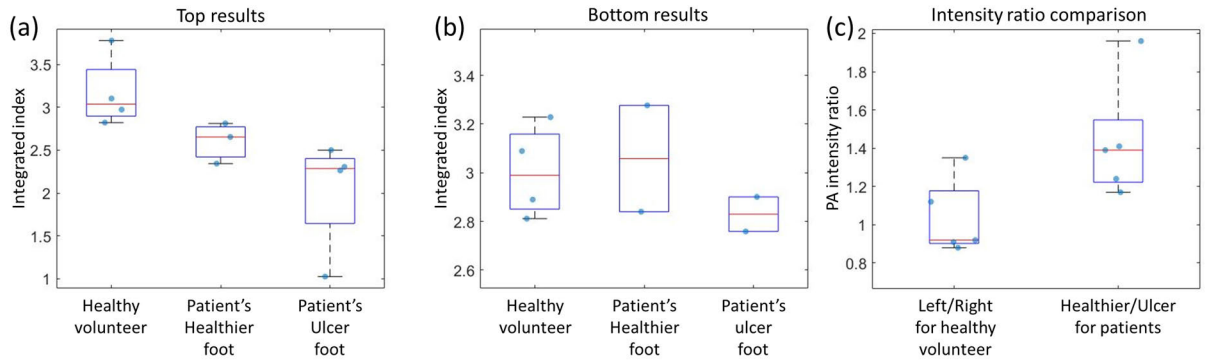

Fig. 10. Quantitative comparisons between healthy volunteers, healthy feet of the patients, and feet with ulcers of the patients for features acquired by the (a) top system and (b) bottom system. (c) Comparison of the PA intensity ratio between healthy volunteers and patients. The ratio is calculated as left/right for healthy volunteers and healthier foot/ulcer foot for patients. Data are presented as box plots and data points are marked.

TABLE III
VESSEL FEATURES EXTRACTED FROM PATIENT 3. THE PATIENT HAS AMPUTATION ON THE LEFT FOOT (MARKED IN RED)

Patient Number	Patient 3			
Foot	Top		Bottom	
	L	R	L	R
PA intensity ratio	1.17		1.41	
Vessel occupancy	0.38	0.38	0.32	0.35
Sharpness x10^2	0.14	0.15	1.90	2.18
Vessel density	2.15	2.20	2.45	2.75
Integrated index	2.33	2.37	2.90	3.28

IV. DISCUSSION AND CONCLUSION

In this study, we developed a dual-scan PAT system to image the vascular structures of the foot and use that information to predict perfusion, which could facilitate clinical decision-making. The top and bottom subsystem design increases the available imaging region and shortens the scanning time. As Fig. 2(b) shows, the current system can cover at least half of the foot, allowing it to handle various ulcer positions. For better scanning of the foot, we implemented several mechanisms, such as the adaptive height adjustment, customized water tank with a slope, and the ball stage for better alignment of the transducer. Moreover, the top and bottom systems can work independently, providing more flexibility for wound imaging.

Compared to the existing cross-sectional PAT system for foot imaging [12], [13], [14], [15], the proposed design utilizes two linear transducer arrays to image the dorsal and plantar sides of the foot simultaneously. Therefore, our system provides a larger field of view. In addition, the scanner is driven by the translation stage, which reduces the motion artifacts from the freehand operation. Compared to other 3-D foot imaging systems, the linear transducer array used in our system has a lower cost [18]. While there are also some linear-array-based 3-D foot imaging systems [16], [17], our proposed design used sterilized ultrasound gel instead of water for coupling. It reduces the imaging preparation time and the risk of cross-contamination between patients.

To better evaluate perfusion condition, we quantified four vessel features: the PA intensity ratio, VO, vessel sharpness, and VD. These features are calculated by an automated algorithm, eliminating the influence of subjective manual operation. The PA intensity ratios are larger than 1 in most patient cases, showing that healthier feet have better tissue perfusion. However, we could not compare the PA intensity among patients as the skin condition and color affects the subdermal optical fluence. A more robust PA intensity measure could be investigated in the future to mitigate the skin effect. We compare the PA intensity ratio among patients (healthier foot/ulcer foot) and healthy volunteers (left/right), and the result indicates that the intensity ratio is close to 1 for healthy volunteers while the result from patients is larger than 1. The integrated index of vessel features proposed in this study provides a single number for easy clinical use. We compared these indices of the healthier and ulcered feet of the same patient and found that the indices are smaller in the ulcered foot in most cases. For better visualization, we upload the indices into box plots. As shown in Fig. 10, the integrated indices of healthy volunteers are larger than that of patients, regardless of the presence of the ulcer. Since peripheral artery disease (PAD) is a systemic disorder, it is likely that the foot without an ulcer also has abnormal perfusion. Among patients, the indices from feet without ulcers are generally larger than that of feet with ulcers, which agrees with clinical observation. Thus, the four vessel features applied in this study have the potential to be used in further clinical studies to predict tissue perfusion. We also noticed that VO and VD show a similar tendency though they indicate different information. The VD represents the number of vessels, whereas the VO demonstrates not only the numbers, but also the volume of the vessels. In comparison to traditional methods such as ABI/TBI tests, the proposed system can obtain information in a specific region close to the wound, allowing clinicians to gain a better understanding of the tissue perfusion. In addition, the ABI/TBI test is sometimes impeded by amputations or other foot conditions, such as in patient 3, while the PAT system can acquire the vessel information in wider clinical conditions.

In this study, a skin removal algorithm has been developed by manually marking the skin boundary along both lateral and elevational cross sections, as the skin pigment plays a

key role in PA imaging quality. The subdermal vasculatures are clearly visible after removing the skin layer as shown in Fig. 3. While we have not recruited any patients with dark skin, we expected that the algorithm will perform well in such patients since the skin signal would be easier to identify. However, the ultimate imaging depth could be affected due to strong skin attenuation. Nonetheless, given that most foot ulcers are superficial, adequate signals for feature extraction and quantification should still be attainable.

While promising results have been demonstrated, further improvements in both hardware and software can be implemented. For the hardware, the water tank design can be improved to fit the shape of the foot better, leading to a large field of view with improved coupling. In addition, the current system uses a flashlamp-pumped laser, which is bulky as it requires water cooling. Diode-pumped lasers [35] can be used to further reduce the system size. Furthermore, multispectral PA imaging can be implemented for the quantification of blood oxygenation, which is also related to perfusion [11].

In terms of software, the calculated PA indices are both system and patient dependent. Variations in system parameters, such as spatial resolution and excitation wavelength, as well as fluctuations in patient condition, would affect the quantification results. A normalization factor can be developed in the future to neutralize these dependencies and make the quantification results more universally applicable. Moreover, advanced image reconstruction and processing methods can be implemented to reduce image noise and improve spatial resolution [36], [37], [38]. Such improvements would allow for a more precise quantification of VO. A cleaner image will also enable the quantification of vessel curvature, which is relevant to perfusion [39]. Finally, the proposed calculation method can be optimized with more clinical data with proper weighting on different indices to provide a more accurate prediction for tissue perfusion. We also plan to include more PAD control patients without foot ulcers to evaluate the potential of our technique for early ulcer detection.

In conclusion, a compact dual-scan 3-D PAT system is proposed in this study. The system can simultaneously image both the dorsal and plantar sides of the foot, leading to a short scanning time. Coplanar light illumination and acoustic detection are achieved on both the top and bottom subsystems to increase imaging depth. In addition, we used an adaptable height scan on the top system to ensure that the feature of interest is always near the transducer focus. The resolution of the system has been quantified with the crossline phantoms. The in vivo results from healthy volunteers indicate that the system can acquire clear images of foot vascular structure in less than 1 min of scanning time. Preliminary results from patients with chronic wounds demonstrate the capability of the system to image the vessels of the patients under different situations. Four vessel features from PA images are extracted for analysis, an integrated index is proposed for easy clinical use, and most of the results correlate with the foot condition. As an ongoing study, more patient data will be added in the future to further enhance the accuracy and robustness of our technique, making it a valuable tool for foot ulcer evaluation.

Declaration of Competing Interest

Dr. Jun Xia is the Founder of Sonioptix, LLC, which, however, did not support this work. All other authors declare no conflicts of interest.

References

[1] Y. Wang, Y. Zhan, L. M. Harris, S. Khan, and J. Xia, "A portable three-dimensional photoacoustic tomography system for imaging of chronic foot ulcers," *Quant. Imag. Med. Surg.*, vol. 9, no. 5, p. 799, May 2019.

[2] C. K. Sen et al., "Human skin wounds: A major and snowballing threat to public health and the economy," *Wound Repair Regener.*, vol. 17, no. 6, pp. 763–771, Nov. 2009.

[3] E. J. Boyko, M. Monteiro-Soares, and S. G. Wheeler, "Peripheral arterial disease, foot ulcers, lower extremity amputations, and diabetes," in *Diabetes in America*, 3rd ed. Bethesda, MD, USA: National Institute of Diabetes and Digestive and Kidney Diseases (NIDDK), 2018.

[4] K. F. Ma, S. F. Kleiss, R. C. L. Schuurmann, R. P. H. Bokkers, Ç. Ünlu, and J.-P.-P. M. De Vries, "A systematic review of diagnostic techniques to determine tissue perfusion in patients with peripheral arterial disease," *Exp. Rev. Med. Devices*, vol. 16, no. 8, pp. 697–710, Aug. 2019.

[5] G. FrykbergRobert, "Challenges in the treatment of chronic wounds," *Adv. Wound Care*, vol. 4, no. 9, pp. 560–582, May 2015, doi: 10.1089/wound.2015.0635.

[6] J. Allen, "Photoplethysmography and its application in clinical physiological measurement," *Physiolog. Meas.*, vol. 28, no. 3, pp. 1–39, Mar. 2007.

[7] M. Venermo et al., "Pilot assessment of the repeatability of indocyanine green fluorescence imaging and correlation with traditional foot perfusion assessments," *Eur. J. Vascular Endovascular Surgery*, vol. 52, no. 4, pp. 527–533, Oct. 2016.

[8] L. V. Wang and S. Hu, "Photoacoustic tomography: In vivo imaging from organelles to organs," *Science*, vol. 335, no. 6075, pp. 1458–1462, Mar. 2012, doi: 10.1126/science.1216210.

[9] J. Xia, J. Yao, and L. H. V. Wang, "Photoacoustic tomography: Principles and advances," *Prog. Electromagn. Res.*, vol. 147, pp. 1–22, Jan. 2014, doi: 10.2528/pier14032303.

[10] N. Settembre, P. Kauhanen, A. Albäck, K. Spillerova, and M. Venermo, "Quality control of the foot revascularization using indocyanine green fluorescence imaging," *World J. Surg.*, vol. 41, no. 7, pp. 1919–1926, Jul. 2017.

[11] G. Saiko, P. Lombardi, Y. Au, D. Queen, D. Armstrong, and K. Harding, "Hyperspectral imaging in wound care: A systematic review," *Int. Wound J.*, vol. 17, no. 6, pp. 1840–1856, Dec. 2020.

[12] J. Yang, G. Zhang, M. Wu, Q. Shang, L. Huang, and H. Jiang, "Photoacoustic assessment of hemodynamic changes in foot vessels," *J. Biophotonics*, vol. 12, no. 6, Jun. 2019, Art. no. e201900004.

[13] J. Yang, G. Zhang, Q. Shang, M. Wu, L. Huang, and H. Jiang, "Detecting hemodynamic changes in the foot vessels of diabetic patients by photoacoustic tomography," *J. Biophotonics*, vol. 13, no. 8, Aug. 2020, Art. no. e202000011.

[14] A. Taruttis, A. C. Timmermans, P. C. Wouters, M. Kacprowicz, G. M. van Dam, and V. Ntziachristos, "Optoacoustic imaging of human vasculature: Feasibility by using a handheld probe," *Radiology*, vol. 281, no. 1, pp. 256–263, Oct. 2016.

[15] Y. Mantri, T. R. Dorobek, J. Tsujimoto, W. F. Penny, P. S. Garimella, and J. V. Jokerst, "Monitoring peripheral hemodynamic response to changes in blood pressure via photoacoustic imaging," *Photoacoustics*, vol. 26, Jun. 2022, Art. no. 100345.

[16] W. Choi et al., "Three-dimensional multistructural quantitative photoacoustic and US imaging of human feet in vivo," *Radiology*, vol. 303, no. 2, pp. 467–473, May 2022.

[17] C. Lee, W. Choi, J. Kim, and C. Kim, "Three-dimensional clinical handheld photoacoustic/ultrasound scanner," *Photoacoustics*, vol. 18, Jun. 2020, Art. no. 100173.

[18] K. Nagae et al., "Real-time 3D photoacoustic visualization system with a wide field of view for imaging human limbs," *FResearch*, vol. 7, p. 1813, Nov. 2018.

[19] S. V. Agale, "Chronic leg ulcers: Epidemiology, aetiopathogenesis, and management," *Ulcers*, vol. 2013, pp. 1–9, Apr. 2013.

[20] L. G. Montilla, R. Olafsson, D. R. Bauer, and R. S. Witte, "Real-time photoacoustic and ultrasound imaging: A simple solution for clinical ultrasound systems with linear arrays," *Phys. Med. Biol.*, vol. 58, no. 1, pp. 1–12, Jan. 2013.

[21] Y. Wang, R. S. A. Lim, H. Zhang, N. Nyayapathi, K. W. Oh, and J. Xia, "Optimizing the light delivery of linear-array-based photoacoustic systems by double acoustic reflectors," *Sci. Rep.*, vol. 8, no. 1, pp. 1–7, Aug. 2018.
[22] D. Tomassoni, E. Traini, and F. Amenta, "Gender and age related differences in foot morphology," *Maturitas*, vol. 79, no. 4, pp. 421–427, Dec. 2014.
[23] M. Xu and L. V. Wang, "Universal back-projection algorithm for photoacoustic computed tomography," *Phys. Rev. E, Stat. Phys. Plasmas Fluids Relat. Interdiscip. Top.*, vol. 71, no. 1, Jan. 2005, Art. no. 016706.
[24] B. Münch, P. Trtik, F. Marone, and M. Stampanoni, "Stripe and ring artifact removal with combined wavelet-Fourier filtering," *Optics Exp.*, vol. 17, no. 10, pp. 8567–8591, 2009.
[25] A. F. Frangi, W. J. Niessen, K. L. Vincken, and M. A. Viergever, "Multiscale vessel enhancement filtering," in *Proc. Int. Conf. Med. Image Comput. Comput.-Assist. Intervent.* Cham, Switzerland: Springer, 1998, pp. 130–137.
[26] K. Zuiderveld, "Contrast limited adaptive histogram equalization," *Graph. Gems*, pp. 474–485, Jul. 1994.
[27] A. Madasamy, V. Gujrati, V. Ntziachristos, and J. Prakash, "Deep learning methods hold promise for light fluence compensation in three-dimensional optoacoustic imaging," *J. Biomed. Opt.*, vol. 27, no. 10, Oct. 2022, Art. no. 106004.
[28] T. W. Ridler and S. Calvard, "Picture thresholding using an iterative selection method," *IEEE Trans. Syst., Man, Cybern.*, vol. SMC-8, no. 8, pp. 630–632, Aug. 1978.
[29] M. Kerschnitzki et al., "Architecture of the osteocyte network correlates with bone material quality," *J. Bone Mineral Res.*, vol. 28, no. 8, pp. 1837–1845, Aug. 2013.
[30] T. C. Lee, R. L. Kashyap, and C. N. Chu, "Building skeleton models via 3-D medial surface axis thinning algorithms," *CVGIP, Graph. Models Image Process.*, vol. 56, no. 6, pp. 462–478, Nov. 1994.
[31] G. Cruz, D. Atkinson, M. Henningsson, R. M. Botnar, and C. Prieto, "Highly efficient nonrigid motion-corrected 3D whole-heart coronary vessel wall imaging," *Magn. Reson. Med.*, vol. 77, no. 5, pp. 1894–1908, May 2017.
[32] A. Shaterian et al., "Real-time analysis of the kinetics of angiogenesis and vascular permeability in an animal model of wound healing," *Burns*, vol. 35, no. 6, pp. 811–817, Sep. 2009.
[33] N. Eizenberg et al., *General Anatomy: Principles and Applications*. Australia: McGraw-Hill, 2007.
[34] T. Sowers, H. Yoon, and S. Emelianov, "Investigation of light delivery geometries for photoacoustic applications using Monte Carlo simulations with multiple wavelengths, tissue types, and species characteristics," *J. Biomed. Opt.*, vol. 25, Jan. 2020, Art. no. 016005.
[35] D. Wang et al., "Deep tissue photoacoustic computed tomography with a fast and compact laser system," *Biomed. Opt. Exp.*, vol. 8, no. 1, pp. 112–123, 2017.
[36] J. Xia et al., "Three-dimensional photoacoustic tomography based on the focal-line concept," *J. Biomed. Opt.*, vol. 16, no. 9, p. 1, Sep. 2011, Art. no. 090505, doi: 10.1117/1.3625576.
[37] H. Zhang et al., "Deep-E: A fully-dense neural network for improving the elevation resolution in linear-array-based photoacoustic tomography," *IEEE Trans. Med. Imag.*, vol. 41, no. 5, pp. 1279–1288, May 2022.
[38] W. Zheng et al., "Deep-E enhanced photoacoustic tomography using three-dimensional reconstruction for high-quality vascular imaging," *Sensors*, vol. 22, no. 20, p. 7725, Oct. 2022.
[39] Y. Matsumoto et al., "Label-free photoacoustic imaging of human palmar vessels: A structural morphological analysis," *Sci. Rep.*, vol. 8, no. 1, pp. 1–8, Jan. 2018.

Chuqin Huang received the B.E. degree in mechanical engineering from the Huazhong University of Science and Technology, Wuhan, China, in 2018, and the M.S. degree in mechanical engineering from the University of Washington, Seattle, WA, USA, in 2020. He is currently pursuing the Ph.D. degree with the Department of Biomedical Engineering, University at Buffalo, The State University of New York, Buffalo, NY, USA.

His research interests include photoacoustic tomography and its application on foot imaging.

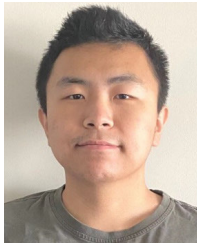

Yanda Cheng received the Bachelor of Science degree in electrical engineering from the University of Kentucky, Lexington, KY, USA, in 2020, and the Master of Science degree in biomedical engineering from Cornell University, Ithaca, NY, USA, in 2021. He is currently pursuing the Ph.D. degree with the Department of Biomedical Engineering, University at Buffalo, The State University of New York, Buffalo, NY.

His research focuses on photoacoustic imaging, deep learning, machine learning, and image processing.

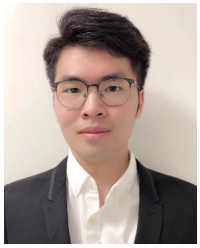

Wenhan Zheng is currently pursuing the Ph.D. degree with the Department of Biomedical Engineering, University at Buffalo, The State University of New York, NY, USA.

He has over ten publications in peer-reviewed journals, specifically focusing on photoacoustics. Furthermore, he has acquired substantial industry experience by working with leading global companies in the field.

Robert W. Bing received the B.S. degree in biomedical engineering with a concentration in nanotechnology from Boston University, Boston, MA, USA, in 2022. He is currently pursuing the Ph.D. degree in biomedical engineering with University at Buffalo, The State University of New York, Buffalo, NY, USA.

His research areas of interest include photoacoustic and ultrasonic sensing.

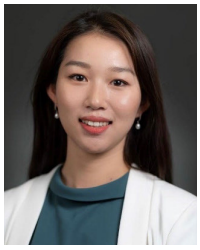

Huijuan Zhang received the Ph.D. degree in biomedical engineering from University at Buffalo, Buffalo, NY, USA, in 2023.

She is a Postdoctoral Fellow at Wellman Center for Photomedicine, Boston, MA, USA, Massachusetts General Hospital, Boston, and Harvard Medical School, Boston. She has published more than 20 papers in peer-reviewed journals on medical imaging research. Her research interests include photoacoustic imaging, deep learning, and optical coherence imaging.

Isabel Komornicki received the bachelor's and Masters of Science in nursing from The State University of New York (SUNY), Buffalo, NY, USA, 1995 and 1998, respectively.

She is with the University at Buffalo Surgeons for the past 16 years in the Department of Surgery, Vascular Department. She is primarily active in the outpatient clinical settings, treating vascular patients in all phases of the disease. She has also participated in numerous research projects throughout her career, involving medical devices, pharmaceuticals, and novel immunotherapies-related vascular and connective tissue disorders. Currently, she is a Research Coordinator with the SUNY at Buffalo Research Foundation, in addition to clinical practice.

Linda M. Harris is a tenured Professor of Surgery with the Department of Surgery, Division of Vascular Surgery, Jacobs School of Medicine and Biomedical Sciences, University at Buffalo, Buffalo, NY, USA. She is the previous Chief of the Division of Vascular Surgery and currently the Program Director for the vascular training programs. She has been practicing in Buffalo for over 25 years since completing her general surgery and vascular surgery training at the University of Buffalo. She has served as the President of the Eastern Vascular Society and the Association of Program Directors in Vascular Surgery. She has coedited two books, written over 20 book chapters, and published well over 100 peer-reviewed publications on a wide variety of vascular diseases. Her research interests include peripheral arterial disease (PAD), including diagnostic assessment.

Praveen R. Arany received the B.D.S. degree in dentistry from Dharwad University, Dharwad, India, in 1999, the M.D.S. degree in oral pathology from Rajiv Gandhi University, Bangalore, India, the M.M.Sc. degree in oral biology, and the Ph.D. degree in dental medicine from Harvard University, Cambridge, MA, USA, in 2011.

He is a tenured Associate Professor in oral biology with adjunct appointments in the Departments of Surgery and Biomedical Engineering. He has certificates in clinical translation and completed postdoctoral fellowships at NCI and Wyss Institute, Boston, MA. He has over 150 peer-reviewed publications and eight book chapters and serves on several editorial boards and policy agencies where he is actively involved with leadership roles. His research focuses on clinical translational biophotonics in tissue healing and regeneration.

Saptarshi Chakraborty is an Assistant Professor of Biostatistics at The State University of New York, Buffalo, NY, USA. His research interests include the theory and applications of computation-heavy statistical methods, big and high-dimensional data analysis, Bayesian modeling, statistics in genomics and computational biology, Bayesian computations and Markov chain Monte Carlo, multivariate analysis, dimension reduction, and statistical methods for medical product safety.

Qifa Zhou (Fellow, IEEE) received the Ph.D. degree from the Department of Electronic Materials and Engineering, Xi'an Jiaotong University, Xi'an, China, in 1993.

He is currently a Professor of Biomedical Engineering and Ophthalmology, the University of Southern California, Los Angeles, CA, USA. He has authored or coauthored more than 260 peer-reviewed articles in journals, including *Nature Medicine*, *Nature Biomedical Engineering*, *Nature Communications*, *Science Advanced*, *Advanced Materials*, and the IEEE TRANSACTIONS ON ULTRASONICS, FERROELECTRICS, AND FREQUENCY CONTROL (UFFC). His research interests include the development of piezoelectric high-frequency ultrasonic transducers/arrays for biomedical ultrasound and photoacoustic imaging, including intravascular imaging, cancer imaging, and ophthalmic imaging. He is also actively exploring ultrasonic-mediated therapeutic technology, including trans-sclera drug delivery and ultrasound for retinal and brain stimulation.

Dr. Zhou is a fellow of the International Society for Optics and Photonics (SPIE) and the American Institute for Medical and Biological Engineering (AIMBE). He is a member of the Technical Program Committee of the IEEE International Ultrasonics Symposium. He is an Associate Editor of the IEEE UFFC.

Wenyao Xu (Senior Member, IEEE) received the B.S. and M.S. degrees (Hons.) from Zhejiang University, Hangzhou, China, in 2006 and 2008, respectively, and the Ph.D. degree from the University of California, Los Angeles, CA, USA, in 2013.

He is a Professor at the Department of Computer Science and Engineering, The State University of New York (SUNY), Buffalo, NY, USA. He published over 230 technical papers, coauthored two books, and was named inventor on nine International and U.S. Patents. His recent research foci include the Internet of Things, smart health, and cyber-security, and his work has received 11 Best Paper Awards in related research fields.

Dr. Xu has served on the technical program committee of numerous conferences in the field of smart health, mobile computing, and the Internet of Things and has been a TPC Co-Chair of IEEE BSN 2018/2023 and IEEE/ACM CHASE 2022.

Jun Xia (Member, IEEE) received the Ph.D. degree in mechanical engineering from the University of Toronto, Toronto, ON, Canada, in 2010.

He held a postdoctoral training in biomedical engineering at Washington University, St. Louis, MO, USA. He is an Associate Professor with the Department of Biomedical Engineering, University at Buffalo, The State University of New York, NY, USA. He has published one book, three book chapters, and more than 90 papers in peer-reviewed journals on optical, ultrasound, and photoacoustic research.